IOP Conf. Series: Materials Science and Engineering **1310** (2024) 012009 doi:10.1088/1757-899X/1310/1/012009

The Metallurgy of Additive Manufacturing: Potentials and Challenges towards Industrialisation

P Mayr[1], S Rauh[1,2], G Matheson[1,3], S Rotzsche[1], S Hartmann[1,4], and E Kabliman[1]

[1]Chair of Materials Engineering of Additive Manufacturing, Department of Materials Engineering, TUM School of Engineering and Design, Technical University of Munich, Freisinger Landstrasse 52, Garching b. Munich, 85748, Bavaria, Germany
[2]Fraunhofer UMSICHT, Fraunhofer Institute for Environmental, Safety, and Energy Technology, An der Maxhütte 1, Sulzbach-Rosenberg, 92237, Bavaria, Germany
[3]Oerlikon AM Europe GmbH, Freisinger Landstrasse 52, Garching b. Munich, 85748, Bavaria, Germany
[4]Siemens AG, Erlangen, Bavaria, Germany

E-mail: evgeniya.kabliman@tum.de

Abstract. The present paper discusses the potential and challenges of processing metallic materials using additive manufacturing. Particular focus is given to laser powder bed fusion (PBF-LB/M) and the use of traditional alloy powders such as Al alloys and Ni-based superalloys, as well as novel materials such as metal-matrix composites. The research includes the improvement of the processability of these alloys using PBF-LB/M and optimizing material properties such as strength, creep resistance, and thermal conductivity of printed parts for various applications. Another important aspect presented within this manuscript is the digital representation of advanced manufacturing systems to improve manufacturability and enable advanced quality control. Herein, the development of a digital twin through in-situ process monitoring for the direct energy deposition process of laser metal deposition is presented. In the last part, the future of materials development for additive manufacturing is discussed, focusing on applying material computational techniques. All demonstrated examples result from the successful cooperation between the Chair of Materials Engineering of Additive Manufacturing, TUM, and its industrial and research partners.

1. Introduction

Additive manufacturing (AM) of metallic components has rapidly developed over the last decades and attracted the interest of scientists and industry simultaneously. Although, this technology has been known for more than 100 years, when the first metal welding techniques were applied to generate 3-dimensional objects, the boom over the last 15 years has resulted in substantial technological advancements in various areas of industry and also our daily lives [1, 2, 3]. Further advantages such as cost reduction, customization, increased part complexity, supply chain optimization, promoting sustainability and circular economy have been discussed widely in the literature [4, 5]. The boom of additive manufacturing, especially with metals, can be seen in the steadily increasing number of published scientific papers. Also, the number of scientific conferences in this area has skyrocketed. From an industry standpoint, many companies have already included AM in their production portfolio. Also, founders see additive manufacturing

as an enabler technology for their start-ups or directly found companies to further develop and promote this new production technology.

While the fantastic opportunities provided through AM have attracted a lot of interest, industrialization is still behind the anticipated growth rate. The reasons for this can be found in various aspects. First, it should not be forgotten that our existing conventional advanced manufacturing technologies, like casting, forging, welding, etc. have developed and been improved over more than a century. Also, AM is a throughout digital technology, and new developments in other sectors like IT, sensing and control, design, robotics, AI, etc. are implemented daily. This, on the one hand, leads to a steady improvement in AM with uncountable possibilities, but on the other hand also gets AM in conflict with traditional manufacturing philosophies, especially quality control. There are still several critical topics that have to be solved to advance AM further. The development of regulatory and legal frameworks, quality assurance and certification, scalability and production efficiency, process control, and standardization, post-processing and finishing, and supply chain integration are just a few but major areas that have to be addressed. Only if the whole value chain of AM is mastered, the casualness and professionalism, known from other advanced manufacturing technologies, will allow the further implementation of AM.

Within this manuscript, research along the process chain of AM, starting with materials development for advanced metallic alloys and improved manufacturability, is presented. The critical role of post-processing and heat treating is shown for a Ni-based alloy used in critical high-temperature applications. How digitalization and simulation can support advancements along the process chain is presented for computational alloy design for AM and the establishment of a digital twin for the directed energy deposition process using a laser beam (DED-LB/M).

2. Laser powder bed fusion of copper-tungsten composites for use in power electronics

Copper-tungsten (Cu/W) composites combine the properties of two metals. The excellent thermal and electrical conductivity of copper (Cu) with the high density, high melting point, and a low coefficient of thermal expansion of tungsten (W). Due to the mutual solid insolubility of Cu and W [6], it is a metal matrix composite (MMC) which is also called a pseudo alloy [7]. These composite materials are used as electrodes for arc welding [8, 9] and for electrical discharge machining (EDM) [10], as high-performance contacts [11] and heat sinks [12, 13, 14]. Commonly Cu/W composites are manufactured by liquid-phase sintering of Cu/W powders compacts or infiltration of porous W skeleton with liquid Cu. However, those processes limit the component geometry and result in costly post-machining [15]. In contrast to this, the powder bed fusion-laser beam (PBF-LB) process can produce components with highly complex geometries. Additively manufactured MMCs can combine multiple properties in a material with a nearly limitless geometry design, tailored to the specific application. So far, MMCs have not been regularly used in industry in the PBF-LB process.

There are several publications on the processing of Cu/W composites by the PBF-LB process. Gu et al. [16] processed a W-20wt%Cu sub-micrometer powder in means of a 2000-watt laser and achieved a relative density of up to 95%. By using a 100-watt laser, Li et al. [17] fabricated building parts with a chemical composition of W–10wt%Cu. Hereby, they measured a relative density of up to 66%. A solution to increasing the densification of Cu/W composite is to use nickel (Ni). However, this leads to a reduction in electrical and thermal conductivity. Such W-Ni-Cu alloys were processed by the PBF-LB process in a few publications [18, 19, 20]. Yan et al. [21] processed several compositions of Cu/W composites with Cu contents of 15-40wt%. They worked with a 200-watt laser system and achieved a relative density up to 98%. They also analyzed thermal conductivity, thermal expansion, roughness, and hardness. Furthermore, there is investigation of the absorptivity of Cu/W powders. The densification of the Cu/W MMC

highly depends on absorptivity of the radiation. Qin et al. [22] determined an absorptivity of 56% for W-20wt%Cu and 51% for W-40wt%Cu at a wavelength of 1070 nm. By using a 500-watt laser, they produced Cu/W composites with a relative density of up to 99.6%. In contrast, Zheng et al. [23] processed Cu/W with low W content of approximately 0.5-2wt%. The Cu/W powder was manufactured in a solution with ammonium tungstate and subsequently reduced through a calcination process. For the Cu-0.5wt%W powder, they measured an absorptivity of 53.1% at a wavelength of 1070 nm. Using a 500-watt laser, they generated test specimens with a relative density of up to 99.5%.

In this study, the processability of copper-tungsten (Cu/W) composites for the PBF-LB process was investigated. A chemical composition of Cu-35wt%W was used. Therefore, sub-micrometer W particles were processed with micrometer Cu particles. The long-term goal is the production of additively manufactured MMC heat sinks for high-performance electronics with a reduced coefficient of thermal expansion to minimize thermal stress in the multi-layer compound. The elements of power device, substrate and heat sink of the multi-layer compound should be able to endure as many heat cycles as possible before failure. Moreover, the MMC should retain high thermal conductivity. Therefore, the process parameters were adjusted to minimize porosity in the test specimen.

2.1. Process setup and characterization methods

MMC powder was processed through a milling process (Pulverisette 5/4, Fritsch). Cu powder with a mean particle diameter (d_{50}) of 25.5 µm and W powders with a d_{50} of 0.7 µm were mixed. 65 wt% Cu and 35 wt% W were weighed in the glove box and modified in a planetary ball mill. To manufacture the test specimens a PBF-LB system (ProX DMP 200, 3D Systems) was used. A maximum laser power of 262 watts, hatch distance of 60 µm, and layer thickness of 30 µm was adjusted. The scan velocity was varied from 500 to 900 mm/s. Argon with 700 ppm O_2 was used as process gas and the specimens were produced on steel plates. Furthermore, a piston reducer (3D Systems) was installed to process reduced amounts of MMC powder. Cuboid samples were manufactured to optimize the process parameters. The scan velocity was varied for the optimization of relative density. Cylindrical specimens were fabricated to analyze thermal conductivity. The relative density was determined optically using light microscopy (Eclipse LV 150, Nikon). The microstructure was analyzed by a scanning electron microscope (JSM-6490, JEOL) and a digital microscope (VHX-2000, Keyence). Thermal diffusivity was measured using laser flash analysis (LFA 457, Netzsch). In addition, the coefficient of thermal expansion was determined using dilatometry (L75 Platinum, Linseis).

2.2. Manufacturing of PBF-LB test specimens and porosity measurements

In figure 1(a), the relative density is plotted as a function of the scan velocity. Incomplete powder layer coverage occurred during the PBF-LB process, leading to the creation of irregular pores due to the lack of material. These types of pores must be differentiated from the lack of fusion porosity, as they are not caused by incomplete melting due to insufficient volume energy density.

The incorrect powder layering could not be eliminated during the experiments. One reason is the poor flowability of the Cu/W composite powder, which hinders a uniform powder layer. According to DIN EN ISO 4490:2018 (Hall flowmeter), the powder is non-flowable. Another negative effect on the powder layer distribution is the application of a piston reducer. Hereby the powder bed is not limited to the sides, in contrast to the standard building plate. The powder can be pushed away from the build plate on both sides during the layering process. In general, powder layering is the dominant factor in the formation of porosity. However, a range from 600 to 900 mm/s as scan velocity can be identified as moderate to manufacture test specimens with high relative density. The experiments also showed that test specimens fabricated in position 1

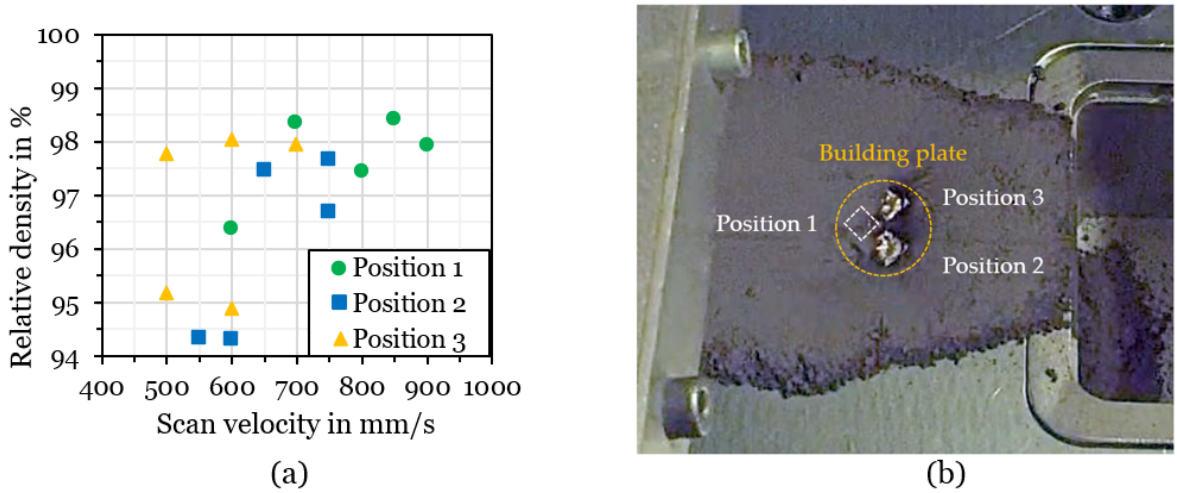

Figure 1. (a) Relative density as a function of the scan velocity; (b) Incomplete powder layering during the PBF-LB process.

had higher relative densities. This position was less affected by incorrect powder layering than positions 2 and 3, as shown in figure 1(b).

2.3. Microstructure

Figure 2(a) shows the microstructure of a Cu-35wt%W composite, analyzed by a scanning electron microscope (SEM). The light grey spots are W and the dark grey area is Cu. Some W particles are melted into phases, surrounded by a Cu matrix. The W phases are separated from the Cu matrix. The distribution of the W phases is heterogeneous. Most of the pores are located between the W phases. The reason could be the high surface tension of Cu. Also, figure 2(b) shows the microstructure of a Cu-35wt%W composite. The grey spots are the W phases and the brown area is the Cu matrix. The black spots are pores.

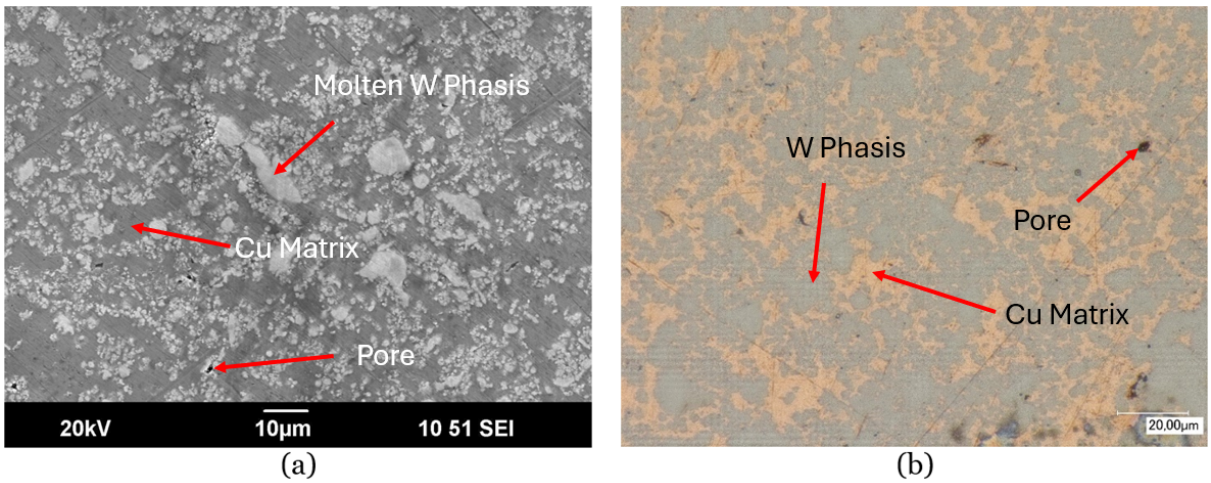

Figure 2. (a) SEM image of Cu-35wt%W composite. (b) Digital microscope image of Cu-35wt%W composite.

2.4. Coefficient of thermal expansion and thermal conductivity

In figure 3(a), the coefficient of thermal expansion (CTE) is plotted as a function of the temperature. The cuboid test specimens, which were measured by dilatometry, are shown in figure 3(b). An average CTE of $14.0 \cdot 10^{-6} K^{-1}$ (at 30°C to 300°C) was achieved with Cu/W composite. The Cu reference specimen had a CTE of $18.1 \cdot 10^{-6} K^{-1}$ (at 30°C to 300°C). In comparison to the Cu reference, the Cu/W composite has a reduced CTE of 22.7%.

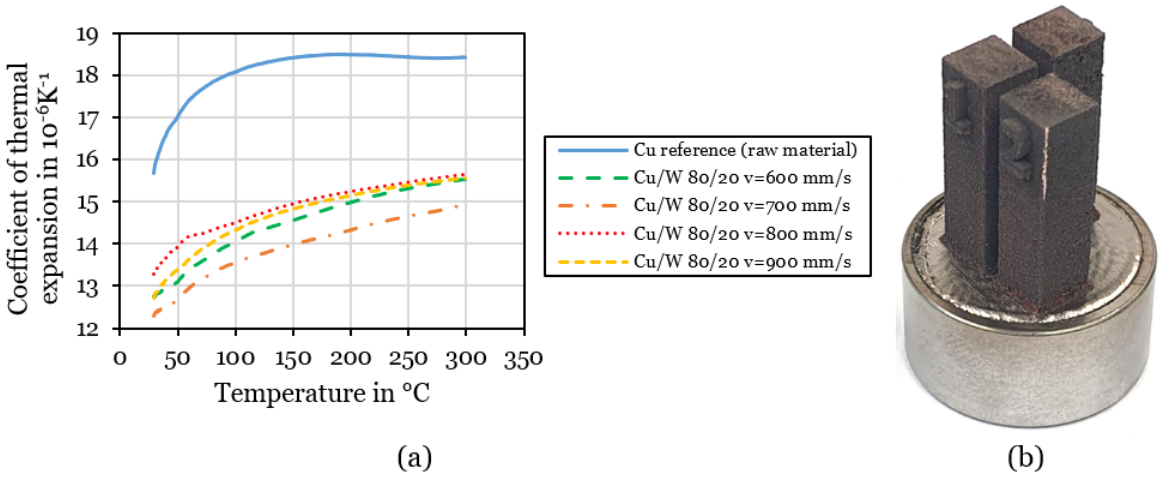

Figure 3. Coefficient of thermal expansion as a function of the temperature (a) measured for the PBF-LB manufactured cuboid test specimens (b).

The thermal conductivity as a function of temperature is shown in figure 4(a). It was measured for cylindrical specimens produced using different scan velocities. The additively manufactured cylindrical test specimen is shown in figure 4(b). As a result, the thermal conductivity of Cu/W composite up to 238.7 W/(m·K) and 396.0 W/(m·K) for the Cu reference was measured. Compared to the Cu reference, a thermal conductivity of 60.3% was achieved.

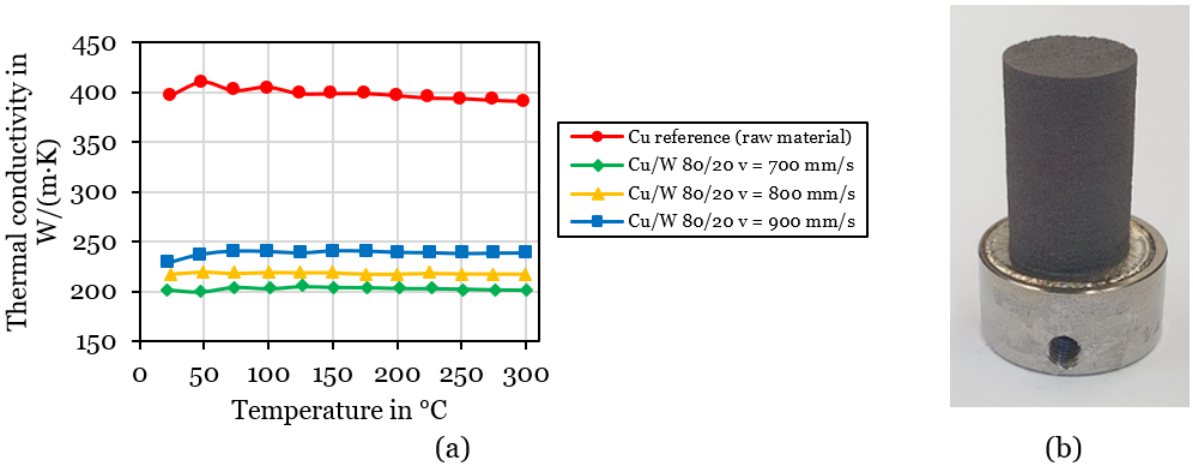

Figure 4. Thermal conductivity as a function of the temperature (a) measured for the PBF-LB manufactured cylindrical test specimens (b).

2.5. Summary and outlook

In summary, a relative density in the range of 96% to 98% was achieved. Furthermore, a coefficient of thermal expansion of $14.0 \cdot 10^{-6} K^{-1}$ (at 30°C to 300°C) was determined. Compared to pure Cu, the thermal expansion coefficient was reduced by 22.7%. Moreover, a thermal conductivity of up to 238.7 W/(m·K) was determined. In comparison to pure copper, 60.3% of the thermal conductivity was retained. Possible measures to increase thermal conductivity by reducing porosity will be implemented. In further experiments, the piston reducer will be removed and samples will be manufactured on the conventional build plate. To increase the flowability of the MMC powder, coarser W powder can be used. After optimizing the process parameters to reduce porosity, demonstrators will be built to show the limits of geometry design.

3. Design of high-strength Al alloys for PBF-LB processing

The rapid solidification rate and complex thermal cycling inherent to the PBF-LB process lead to notably different microstructures in metal alloys compared to cast or wrought material with the same composition.[2] Particular characteristics of the rapidly cooled material are the presence of non-equilibrium phases, fine microstructural features, and a supersaturated matrix [24, 25]. These unique solidification conditions provide major challenges related to cracking but also opportunities related to improved heat treatments when adapting high-strength Al alloys to the PBF-LB process.

3.1. Process induced cracking and routes to printability

In traditional high-strength aluminum alloys such as the age hardenable Al-Cu (2xxx series), Al-Mg-Si (6xxx series), and Al-Zn-Mg (7xxx series) systems, directional solidification in PBF-LB leads to columnar grained microstructures susceptible to intergranular hot tearing [26, 27, 28] This results in parts that are industrially useless due to the high crack density and poor mechanical properties. Strategies to reduce the formation of columnar grains and eliminate cracking are based either on the modification of the processing parameters to reduce thermal gradients, or modification of the chemical composition to refine the grain structure. Heating the building platform to 500°C has been shown to eliminate cracking in the AA6061 alloy [29] while both slow scan speeds [30] and laser defocusing [31] have been used to successfully fabricate crack-free 2xxx series material. However, these processing methods present major limitations for industrial adoption due to low productivity and powder degradation concerns. Modification of the chemical composition to induce a fine equiaxed grain structure, particularly via the introduction of grain refining elements or particles such as Sc, Ti, Zr, TiB2, is a promising solution to render these known alloy systems printable [25]. For example, figure 5 shows the powder feedstock and PBF-LB processed microstructure of AA7075 with and without the addition of 1.2 weight percent titanium (Ti) particles smaller than 25 micrometers via powder blending. A crack-free equiaxed grain structure formed in the printed material following the addition despite incomplete Ti melting seen in figure 5(f). The Ti addition takes the alloy out of standard industrial specification ranges for AA7075 chemical composition and therefore can be considered a new design for PBF-LB Al alloy. Blending powders is a useful way to screen new compositions, but the added process step, more complex powder recycling, and the presence of inclusions lead the industry to prefer pre-alloyed powders.

3.2. Heat treatments of high strength PBF-LB Al alloys

The typical heat treatment for age-hardenable wrought and cast high-strength Al alloys is a two-stage sequence notated as T6 when peak mechanical properties are achieved [32]. The first step is a solution heat treatment meant to dissolve alloying elements into a solid solution, followed by water quenching to trap solutes in the Al matrix. An aging step at a lower temperature is then performed to allow nanometric secondary phase precipitation from solid solution resulting

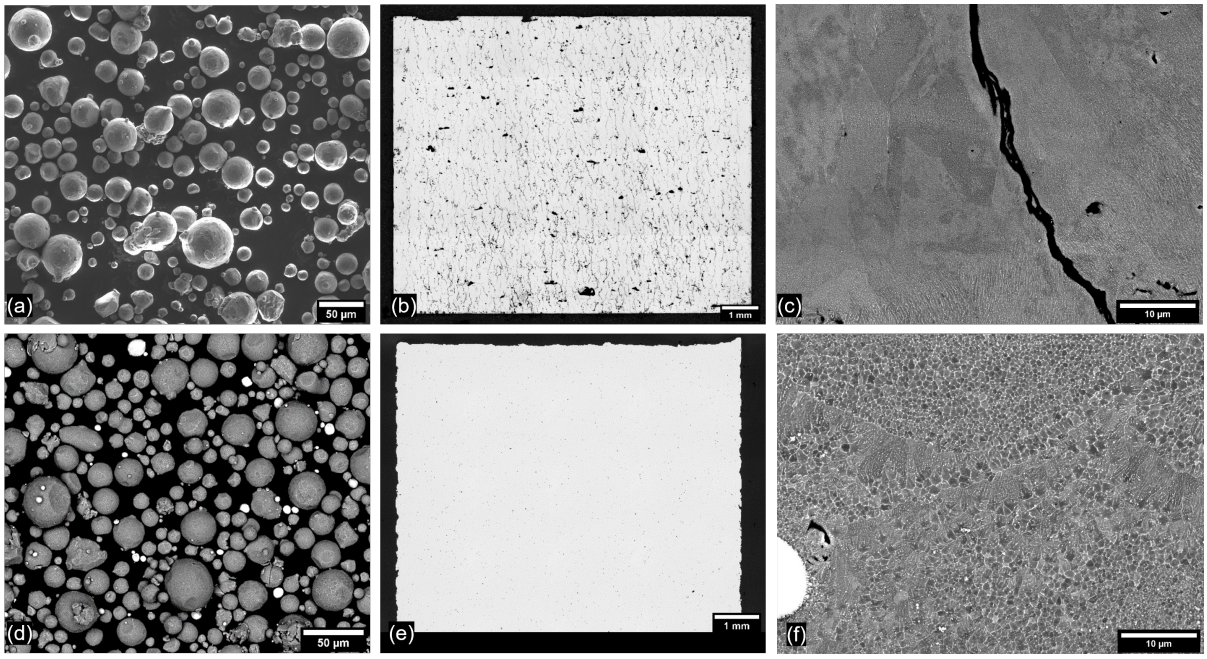

Figure 5. AA7075 powder and bulk micrographs (a,b,c) with no addition and (d,e,f) with 1.2 wt% titanium particle addition.

in hardening. These T6 heat treatments were developed for traditionally fabricated Al material with lower solidification rates than occur in PBF-LB, and where a solution and quenching operation is necessary to obtain a saturated solid solution. The as-built microstructures of PBF-LB Al alloys already have a supersaturated matrix and therefore require novel heat treatments to reach optimized mechanical properties [33]. Moreover, a solution heat treatment step can coarsen fine grains, and result in coarser precipitates which harm the mechanical properties compared to the as-built microstructural state [25]. Direct aging - a single-step heat treatment, notated as T4, to relieve residual stress and trigger precipitation is generally found to be a better choice for PBF-LB Al alloys [34, 35, 36]. Moreover, skipping the water quenching step in the standard T6 reduces risk for industrial users. Since PBF-LB is a near-net shape manufacturing technique that often takes advantage of complex features and thin walls, water quenching can cause unacceptable geometric distortion in critical components.

In the case of the AA7075 alloy with blended Ti additions shown in figure 5, uniaxial tensile testing was performed on samples in the as-built, T4 and T6 heat treatment cases shown in figure 6. The single-step T4 heat treatment resulted in increased mechanical properties (413MPa yield strength, 6.7 % elongation) compared to the T6 heat treatment (373 MPa yield strength, 5.8 % elongation), These results illustrate that direct aging treatments can provide superior mechanical properties than standard two-step heat treatments on grain refined AA7075. Heat treatment optimization needs to be conducted for each alloy based on its as-built microstructure. Such optimizations should be aided by kinetic modeling of precipitate phases as described in section 6 of this paper.

3.3. Summary and outlook

In summary, adapting crack-susceptible high-strength Al alloys to PBF-LB via the addition of grain refiners is an effective solution to solve the cracking challenge - demonstrated here with the AA7075 alloy rendered printable via the blending of 1.2 wt% Ti particles into the feedstock

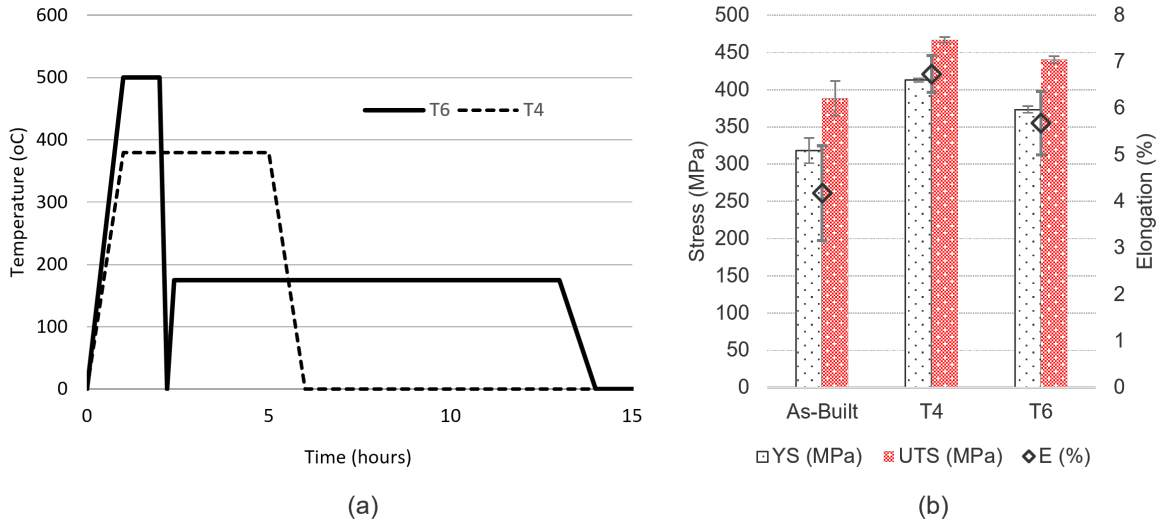

Figure 6. Holding temperatures and duration of T4 and T6 heat treatments applied to AA7075 + 1.2 wt% Ti particles (a) associated yield strength, ultimate tensile strength and elongation at break in the as-built and heat treated conditions (b).

powder. The particularities of the AM microstructure mean that traditional heat treatments are not well suited for these alloys and new heat treatments must be developed to take advantage of the processing technique.

4. Optimization of heat treatment for creep-resistant Ni-based superalloys

Due to the wide range of possible applications in the field of AM, many research questions regarding the process and materials remain unanswered. This section investigates the specific challenges of developing AM alloys for high-temperature applications. In particular, we focus on IN738LC alloy and its modification to improve the processability when using PBF-LB/M.

4.1. Challenges of AM in high-temperature applications

The main challenge of using AM in high-temperature applications lies in the following aspects. It begins with a question on the transferability of existing alloys typically used in conventional manufacturing such as casting or welding for AM including their processability and the quality of the final components. In particular, the resulting microstructure of AM components is typically characterized by elongated grains with a small width-to-length ratio that has a detrimental effect on high-temperature properties such as creep. It can be explained by the fact that grain boundaries exhibit higher diffusion rates of alloying elements resulting in grain boundary sliding at elevated temperatures. Thus, minimizing the fraction of grain boundaries in AM components is essential to enhance resistance against creep. It can be achieved by creating a coarse, equiaxed grain structure to mitigate these effects. In conventional casting processes, grain size can be controlled within the range of several hundred μm to mm by adjusting the casting temperature and preheating the mold. Additionally, resistance against creep can be enhanced through post-heat treatment by adjusting the distribution of the precipitation particles, their size, and morphology. IN738LC alloy, in particular, possesses its high-temperature resistance through a bimodal distribution of primary (cubic) and secondary (spherical) γ' precipitates of $Ni_3(Al,Ti)$ achieved by applying a standard heat treatment consisting of solution annealing at 1120°C for 2 hours (AC) followed by aging at 850°C for 24 hours.

Further insights into the application of conventional alloys in AM can be reached by analyzing their weldability, given the similarity of the respective processes. Alloys used in high-temperature industrial applications, such as CM247LC, and IN738LC, are generally considered difficult to weld [37]. This difficulty is reflected in the AM process by the increased formation of hot cracks and pores during the build process, which can be mitigated, for instance, by altering the chemical composition of the alloy. Unlike casting, where post-process grain coarsening through heat treatment is unnecessary, the resulting grain size from the PBF-LB/M process is in the low micrometer range with a high aspect ratio, coupled with strong grain texturing along the $< 001 >$-direction. Consequently, additional heat treatment is required for AM components to achieve grain coarsening and equiaxed grain orientation, ensuring isotropic mechanical properties. However, applying the aforementioned standard heat treatment to AM components does not lead to grain growth in IN738LC due to the restriction of grain boundary migration by finely precipitated metal-carbon (MC) carbides. This phenomenon is attributed to the Zener pinning effect, which is enhanced by the fine, dispersed precipitation of MC carbides.

4.2. Promoting grain growth in IN738LC alloy

To promote grain growth in additively manufactured IN738LC components, heat treatment at higher temperatures (around 1200°C) and dwell times of several hours is currently applied (see table 1). Upon heating the sample above 1200°C, MC carbides partially dissolve or grow depending on their initial size after the build process [38]. Consequently, the number of carbides, and thus the Zener pinning force, is minimized, facilitating grain growth [38, 39]. Another approach is the transformation of the metastable MC carbides to $M_{23}C_6$ carbides by applying a two-step heat treatment of 950°C for 24 hours followed by 1230°C for 10 hours. This results in a grain enlargement of approximately 400% [39, 40]. Herein, MC carbides are transformed into $M_{23}C_6$ carbides in the first heat treatment step through carbon diffusion along the grain boundaries. In the second step, when the temperature is raised to 1230°C, the $M_{23}C_6$ carbides are dissolved, and coarse MC carbides with a lower density are formed. Thus, the Zener pinning force is reduced allowing for further grain growth [39]. Finally, Peachey et al. [41] demonstrated that also directional recrystallization on AM samples can produce coarse grains with lengths of 650 µm and widths of 150 µm. In this process, rod material is drawn from a cooled zone through a hot zone. However, this method presents a disadvantage compared to furnace heat treatment as it severely restricts component geometry, thus offsetting the advantages of AM.

Table 1. Various strategies of post heat treatment applied to IN738LC after PBF-LB/M.

Heat treatment	Average grain size
1195°C, 6 hours	<60 μm [38]
1245°C, 6 hours	86 μm [38]
1230°C, 10 hours	$\sim$ 40 μm [39]
950°C, 24 hours + 1230°C, 10 hours	$\sim$ 100 μm [39]

4.3. Modification of IN738LC alloy and its heat treatment

The processability of conventional alloys can be enhanced through the modification of their chemical compositions. In this paper, we investigate the IN738LC alloy whose original chemical composition [42] was modified by the addition of 4 wt.% Fe to minimize susceptibility to hot cracking (see table 2) during PBF-LB. The resulting alloying alloy composition demonstrated a hot cracking index of 1.03 and could be manufactured with less than 1 $\frac{Crack}{mm}$ depending on the

process parameters on an unheated substrate plate. The samples were additionally subjected to hot isostatic pressing (HIP) to close residual pores and microcracks as well as to reduce the risk of crack propagation when applying a heat treatment (950°C, 24 hours + 1230°C, 10 hours).

Table 2. Nominal chemical composition of modified IN738LC in wt.% [43]

Cr	Al + Ti	Co	Fe	W	Mo	Ta	C	Ni
16	7	9	4	3	2	2	< 0.1	Bal.

Figure 7 illustrates the optical micrographs of as-built and HIPed samples before and after the heat treatment. Using the line intercept method according to ASTM-E112, grain sizes of 25 μm and 165 μm were determined for the as-built and as-heat-treated samples, respectively. The grain size after the HIP treatment was determined to be 29 μm, and subsequent heat treatment resulted in a grain size of 98 μm. As can be seen, grain growth was observed for both as-built and HIPed samples. However, the percentage of grain growth was significantly lower in samples that have undergone HIP treatment. This is attributed to the fact that the preceding HIP treatment reduces the driving force for grain growth, as it removes the stored internal energy stemming from the building process. To tailor the optimal precipitate distribution after the grain growth, the standard heat treatment (1120°C, 2 hours (AC) + 850°C, 24 hours) for IN738LC should be applied after the 2-step heat treatment (950°C, 24 hours + 1230°C, 10 hours) required for grain growth.

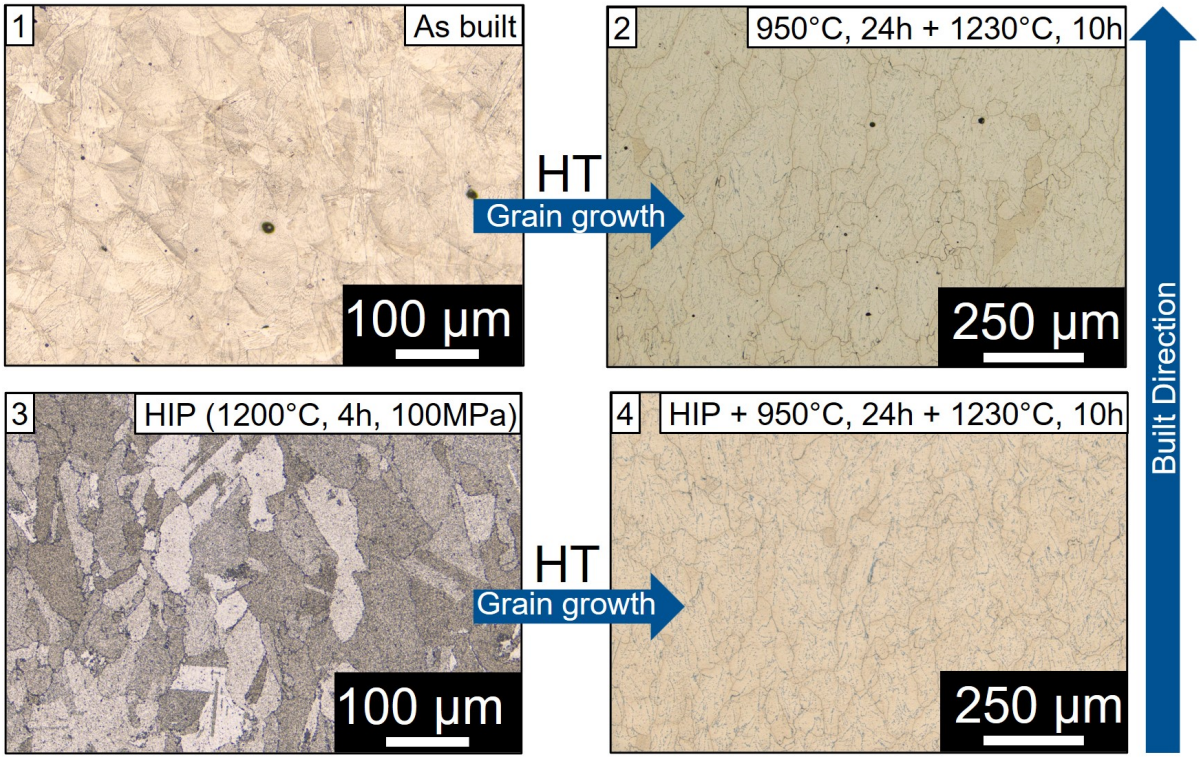

Figure 7. Optical micrographs of (1) as-built sample, (2) as-built + heat-treated sample, (3) HIPed sample, (4) HIPed + heat-treated sample.

4.4. Summary and outlook

The current study demonstrated that high-temperature alloys fabricated by AM, particularly PBF-LB/M, must undergo a post-heat treatment to optimize creep properties by promoting grain growth. The typical temperatures for IN738LC exceed 1200°C. It is associated with the dissolution or transformation of MC carbides and facilitates effective grain growth in PBF-LB/M fabricated samples, leading to increased grain boundary mobility. In particular, the 2-step heat treatment at 950°C for 24 hours + 1230°C for 10 hours presents a viable solution, although with a total duration of 34 hours, posing a significant time factor for industrial applications. Further research questions remain to be investigated, such as detailed investigations of the influence of HIP treatments on grain growth and the addition of 4 wt.% Fe on long-term creep properties.

5. Towards digital twins through in-situ process monitoring

As mentioned above, the extreme physical conditions during metal AM lead to unexpected process results. For DED-L, these anomalies can result in porosities, distortions, and lack of fusion amongst other defects in the final part [44]. A better understanding of the process-structure-property relationship is generally viewed as the most promising possibility to address these persisting issues for DED-L [45].

5.1. Digital Twins

Digital twins (DTs) can help to improve this understanding by using a virtual representation of the respective physical entity [46]. Such virtual representations should combine physics-based simulations to model the behavior of the real object while updating its state based on data derived from the real entity [47]. Applied to manufacturing processes, DT can lead to increased transparency about the respective processes while improving its resilience and flexibility via data-based process adjustments [48]. In the case of metal AM, Gaikwad et al. [49] pointed out that the most significant process improvements can be expected when physics-driven predictions and in-situ anomaly detection from process data are combined within one DT framework.

5.2. Digital Twins in DED-L

Multiple research efforts have already presented approaches towards such a DT framework for DED-L. The work of DebRoy et al. [50] opened the field for DTs in AM. They also proposed a potential use case for DED-L where they showcased how a DT can be employed to reduce the amount of trial and error tests inherent with this technology at the moment. Gaikwad et al. [49] utilized machine learning to fuse physical simulation data with in-situ monitoring data. In their conclusion, the authors pointed out that the prediction accuracy of a DT is enhanced by combining simulation and monitoring data. Regarding the simulation data, Mukherjee and DebRoy [51] highlighted the necessity of a precise mechanistic simulation model and outlined the parameters that such a model should be capable of predicting. With regards to the monitoring data, Gunasegaram et al. [52] deemed a proper validation of the developed DT crucial for obtaining reliable process predictions. In this regard, the works of Hartmann et al. [53] and Chen et al. [54] demonstrated the applicability of combining data streams from multiple sensors with the Tool Center Point (TCP) of the DED-L nozzle. Based on this applicability, another work by Hartmann et al. [55] proposed a more sophisticated monitoring framework based on an edge-cloud computing methodology to systematically create, store, and analyse digital representations of DED-L manufacturing processes. With such a DT of the actual manufacturing process, anomalies can be spotted in situ and location-based correlations between part defects and process faults can be realized. Other examples of applying DTs in DED-L include the work of Zou et al. [56] who measured strain and temperature profiles by embedding fiber optic sensors in an Inconel deposition. The monitoring data was compared to a DT model based on FEA yielding errors of less than 10%. Another research work was published by Hermann

et al. [57], where the authors showcased the first DT framework combining data-driven and physical simulation models to predict the geometry of single tracks. Karkaria et al. [58] also used a data-driven model based on a recurrent neural network to predict temperatures during DED-L deposition in real time. The predictions were then used to adapt the printing process based on Bayesian optimization, but the approach was not tested on a physical DED-L system. Feng et al. [59] proposed a methodology for creating a DT for DED-L. The authors dissect the creation process into different steps starting with the virtual assembly of the equipment, the motion settings, collision inspection, and PLC debugging. However, their work is limited to only providing a concept without testing it with real experiments. The same limitation is valid for the research work conducted by Figueroa et al. [60] who presented a DT concept that was based on the ISO-standard 23247. Their concept combined a KUKA robot with a Meltio deposition head and used IoT tools and protocols to collect and visualize the process data in real-time. While presenting a sophisticated data architecture, their efforts also did not include an experimental use case collecting real data from a real DED-L system.

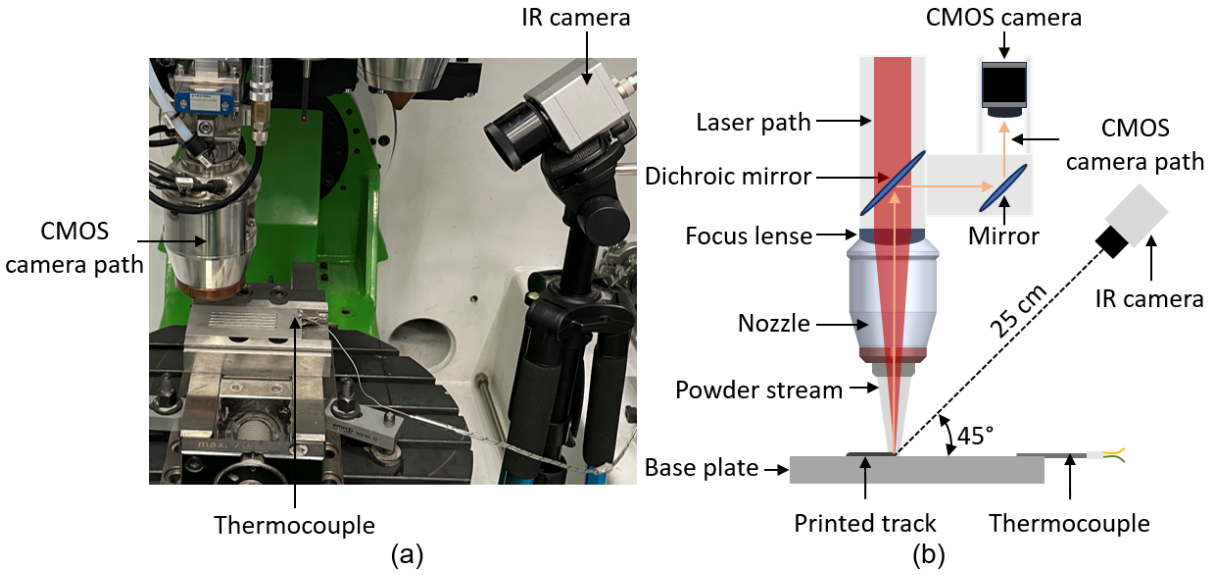

Figure 8. Monitoring setup: (a) employed sensor systems inside of the building chamber, and (b) schematic front view of the monitoring setup (reproduced from [53]).

5.3. Digital Twin validation through in-situ process monitoring

Upon reviewing the literature in the field of DTs, it becomes evident that proper validation with in-situ data coming from physical systems can be very beneficial for the creation of accurate DTs. For DED-L, however, there is a notable absence of such validations in the published research works. To address this gap, Hartmann et al. [53] presented a DT approach, where they compared DT data coming from a multiscale simulation model with in-situ monitoring data from an industrial-grade DED-L system. The monitoring setup included a CMOS camera capable of capturing grayscale images of the melt pool through the optical channel, as well as an off-axis IR camera measuring the temperature of the melt pool. In addition, a thermocouple that constantly measures the temperature of a fixed position was mounted onto the baseplate during the experiments. Inconel 625 powder was used as feedstock material and was melted onto a stainless steel 304 base plate with 100x50x10 mm^3 in dimensions. The experimental setup can be viewed in figure 8.

The sensors were integrated into a BeAM Modulo 400 that was equipped with a SINUMERIK ONE controller and an Industrial Edge IPC to collect the data from the machine and sensors. All data streams were fused so that each position during the build job held information about the respective laser power, feed rate, and sensor values measured. An example following this geo mapping approach can be seen in figure 9. The melt pool width, obtained by the grayscale camera, is depicted for an experiment where five tracks with different process parameters were deposited. The monitoring data is used to validate the DT by comparing its simulation results of the melt pool temperature and width with the IR camera and CMOS camera respectively. Moreover, the capability of the DT to calculate the heat dissipation throughout the build plate is tested with the thermocouple for one fixed position during the experiments. As the DT is also capable of calculating the final deposition's width, height, and cooling rate, metallographic inspections were carried out for the first two experiments to assess those parameters.

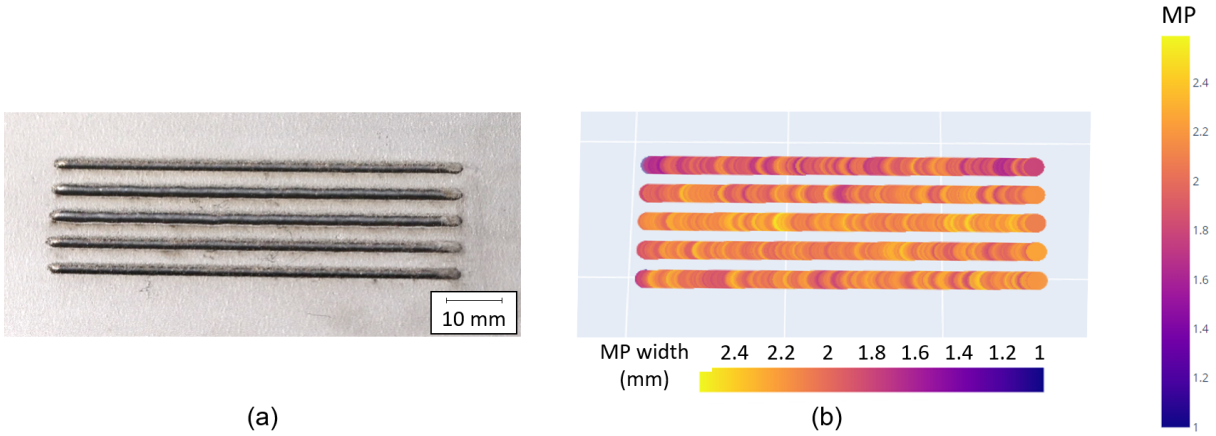

Figure 9. Comparison between the (a) real process part and (b) the geo mapping of the sensor data (reproduced from [53]).

In total, four experiments were defined to test the DT with in-situ monitoring and metallographic data. At first, a five-track sample with varying process parameters was printed twice with different void movement velocities to test the DT's capability for varying process parameter sets and heat dissipation dynamics. For these first two experiments, metallographic data was also obtained via multiple cross-sections to measure the width and height of the clads' cross-sections taken at multiple positions as well as the secondary dendrite arm spacing that correlates with the cooling rate after the deposition process. For the in-situ monitoring data, the DT's average errors were 4.62% for the melt pool temperature, 4.04% for the melt pool width, and 3.75% for the heat dissipation measured with the fixed thermocouple. For the metallographic inspections, the average errors amounted to 4.29% for the clad width and 6.98% for the clad height.

As the DT is also capable of calculating the secondary dendrite arm spacing (SDAS) during DED-L, the evaluation of its accuracy is done via analysis of the microstructures of the produced parts. The SDAS provides valuable information about the cooling rate of the solidification during DED-L. The cooling rate is an important factor influencing the microstructural and mechanical properties of the DED-L-produced parts. In the DT framework, the SDAS is employed to quantify the cooling rate and can be measured in the final parts. Figure 10 depicts the comparison between the simulated and actual SDAS representation.

A total of 16 individual measurements of the SDAS were carried out with a Leica DCM-3D microscope after a Krailing 2 agent was applied to each polished clad. The spacing between the

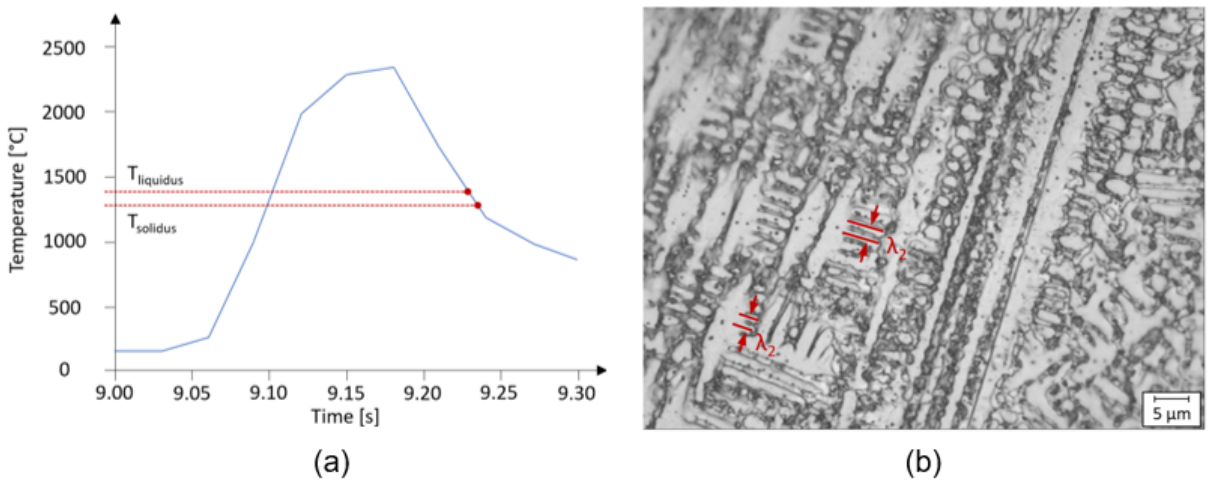

Figure 10. (a) Simulated CR for the SDAS calculation of clad 2.3 and (b) SDAS representation in the metallography of clad 2.3. (reproduced from [53]).

secondary dendrite arms of each sample is compared to the predictions of the DT. The maximum error of 0.36 µm can be deemed acceptable while the average error of 0.018 µm indicates highly precise predictions of the DT.

The validity of the DT for single-clad depositions was hereby ensured. To assess whether the DT is also capable of simulating error-prone build strategies in DED-L, a U-shape and a single-track wall consisting of five layers were chosen as the third and fourth experiments. Here, the in-situ monitoring data was assessing the DT accuracy for the melt pool temperature, dimension, and overall heat dissipation. The average errors amounted to 7%, 4.5%, and 6.19%, respectively.

5.4. Summary and outlook

The systematic collection of in-situ monitoring data enabled a scientific assessment of the predictive capabilities of the proposed DT for DED-L. Moreover, the fusion of sensor and machine data facilitated this assessment by directly comparing spatiotemporal positions within the DT simulation with their corresponding counterparts during the production process. As a result, the DT can be utilized to predict the essential parameters before the manufacturing process. By that, extensive trial-and-error cycles caused by a switch in process parameter sets or manufacturing geometries can be minimized. The capabilities of the DT will be further assessed for more complex geometries and different materials.

6. Computational alloy design for additive manufacturing

The future of materials design involves the intensive application of computational techniques and material models that allow predicting the material properties based on theoretical backgrounds from many disciplines like chemistry, physics, materials science, and engineering. The ability to simulate the manufacturing process and predict the material's properties using virtual (computational) tools can drastically reduce the use of resources such as raw materials and speed up the development process avoiding the time-consuming experimental trials. The requirement is, however, the application of time-efficient computational techniques.

6.1. CALPHAD and its application to AM

Among a large variety of computational materials science methods, which are used to describe the material's behavior, at various time scales, the calculation of phase diagrams known as CALPHAD [61] has found a wide application in many areas of metal manufacturing, including AM [62]. Using CALPHAD, it is possible to theoretically predict the phases and their fractions that can precipitate in multi-component multi-phase materials such as metallic alloys [63]. It is based on the minimization of the Gibbs free energy which is written in the special form accounting for molar Gibbs energies of individual phases as well as configuration effects and physical contributions. Since its development, CALPHAD has been implemented in many open-source and commercially available software such as OpenCalphad, PanDat, Thermo-Calc, and MatCalc to name a few.

When being applied to additive manufacturing, several specifics of the process should be considered. First of all, rapid solidification where cooling happens under non-equilibrium conditions. Thus, the equilibrium state conditions commonly assumed in CALPHAD do not apply here. Alternatively, the Scheil-Gulliver equation can be used which assumes infinite diffusion in the liquid state and restricted diffusion in the solid state. The next challenge is that during AM the already deposited layers are repeatedly heated by the addition of the upper layers. It leads first to the remelting of the underlying layers, and then to the heat treatment of the already solidified layers. This results in the cooling having a non-linear form. Finally, to achieve the target material property values (e.g. strength) the post-heat treatment of the as-built state is often required. This leads to a very complex thermal treatment of the material that is schematically illustrated in figure 11(a). While the solidification step can be approximated using the Scheil-Gulliver approach, special kinetic models are required to calculate the phase fractions in the solid state. These steps should be combined in such a way that the outcome of the Scheil-Gulliver calculation is an input for the kinetic modeling in the solid state.

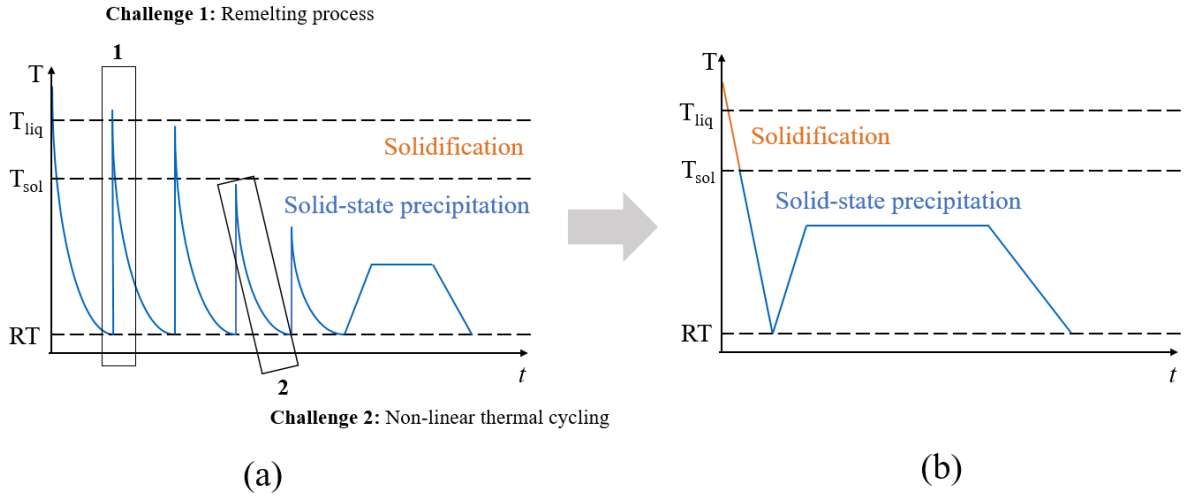

Figure 11. Schematic representation of thermal treatment during additive manufacturing (a) and its common simplification during the CALPHAD modeling (b).

The knowledge of the time-temperature history for each deposition layer or specific sample area is crucial for the correct prediction of phase precipitation in additively manufactured metals. Obtaining this data is, however, not trivial. Therefore, the intrinsic cyclic heat treatment is often approximated by a single-step rapid cooling requiring only a single Scheil-Gulliver calculation (see figure 11(b)).

6.2. CALPHAD-based high-throughput screening

The other strength of the computational materials modeling, e.g. CALPHAD, is the ability to be combined with the high-throughput screening to test many variations of chemical compositions and process parameters. In particular, in AM, several uncertainties can influence the material quality in the end. For instance, the uncertainty in the feedstock material can result in different quality of the final part depending on the supplier [64]. The other challenge is to find the optimal heat treatment of the as-built samples to reach the target material properties (e.g. strength values). While the experimental investigation is usually limited in the number of trials and associated costs, the computational screening is limited mainly by the available computational power. Otherwise, hundreds to millions of combinations can be tested. To do such high-throughput screening, special tools are required. At the Chair of Materials Engineering of Additive Manufacturing, we are developing a tool called CAROUSEL - an open-source framework for high-throughput microstructure simulations [65]. The tool uses MatCalc [66] as the CALPHAD implementation and offers such features as open-source implementation, scripting tools, graphical user interface, task distribution system, data management, and data visualization. Using CAROUSEL, we can perform multiple CALPHAD-based calculations of a different type: equilibrium, non-equilibrium (Scheil), and kinetic simulations as well as combine different steps to realize the through-process modeling.

Figure 12 demonstrates the results of the screening performed for 705 combinations from chemical composition values and heat treatment conditions (temperature, duration, time) for a post-heat treatment of Al-Mg-Si-Ti-Fe alloy after PBF-LB. For simplicity, we restricted the selected phases to the liquid, fcc (Al), Mg_2Si_B, and Al_3Ti_L which were of the most interest for the present study. During the post-heat treatment, it is expected to generate the nano-scale particles that contribute to the strength, herein the secondary Al_3Ti_L particles. However, no precipitation was observed in the calculation confirmed by the experimental measurements that could detect only the coarsening of the secondary Mg_2Si_B particles. This effect was confirmed by computational screening as demonstrated in figure 12. While increasing the holding time at 500 °C, the amount of the secondary Mg_2Si_B increased due to the increase of their mean radius. At the same time, while decreasing the heat treatment temperature from 550 °C to 350 °C, the amount of these particles decreased. Herein, each point on the graph is the result of a single combined calculation using the Scheil-Gulliver equation for solidification and kinetic models for the precipitation in the solid state.

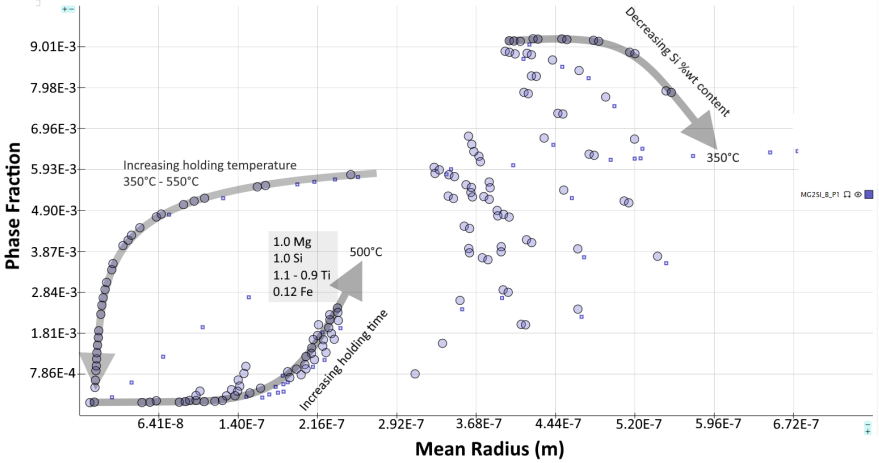

Figure 12. Calculated phase fractions vs. mean radius (reproduced from [65]).

6.3. Summary and outlook

CALPHAD and CALPHAD-based models offer an effective methodology for fast theoretical prediction of the microscopic properties of the materials during AM. Combined with the high-throughput approach, this method opens the opportunity for a rapid design of novel materials and optimization of the related process parameters. However, one should be aware of the shortcomings in both the methodology and application of the CALPHAD to AM. In particular, the available thermo-dynamic databases should be critically evaluated since they were historically validated for manufacturing processes rather than AM. This requires some prior knowledge of the investigated system since simulation with all phases from the database can lead to numerical issues and an inability to find the global minimum. Finally, the process specifics should be taken into account such non-equilibrium conditions.

7. Summary and conclusions

This manuscript presented the results of several successful research activities at the Chair of Materials Engineering of Additive Manufacturing of TUM in cooperation with industry and research partners. The main focus of the chair research strategy is the development of structure-process-property relationships for advanced metallic materials and various additive manufacturing processes. For example, the successful processing of CuW metal matrix composites for power electronics applications using laser powder bed fusion (PBF-LB/M) was demonstrated. It was possible to produce relatively dense parts (98%) with a reduced coefficient of thermal expansion and retaining a good thermal conductivity of 60% compared to pure copper. The improved absorbance of the laser beam's energy for the CuW-alloy system allows additive manufacturing of almost dense CuW parts. The CuW MMC, in combination with the advantages of additive processing, will allow many new applications in power electronics.

Additive manufacturing using PBF-LB/M offers many benefits. However, the intrinsic ultra-fast thermal cyclic heat treatment can result in high porosity and cracking of susceptible alloy systems, such as high-strength aluminum alloys. Within this manuscript, the potential of modifying conventional Al-alloys, including grain-refining elements such as 1.2 wt% titanium, was shown. Crack-free parts with good mechanical properties based on an ultra-fine microstructure have been printed. It was shown that classical heat treatments to improve mechanical properties, such as a T6 heat treatment consisting of solution annealing and aging, can be detrimental to parts produced using PBF-LB/M. The solution annealing leads to significant grain coarsening and inferior mechanical properties. It can be concluded that for additive manufacturing, not only does the chemical composition of alloys have to be adjusted, but special heat treatment cycles also have to be developed as was demonstrated also for the Ni-based superalloys. Additive manufacturing of these materials for high-temperature applications using PBF-LB/M has attracted much interest. However, the application of traditional Ni-based alloys used for forged parts creates problems in additive manufacturing. Aside from a strong susceptibility to hot cracking during printing, PBF-LB/M results in large columnar grains, which result in strong anisotropy of mechanical properties and reduced creep resistance. Here, it was shown that for the alloy IN738LC, special heat treatment procedures must be developed to promote grain coarsening and improve creep properties.

Furthermore, additive manufacturing is a fully digital technology that goes from the design step to the final quality assurance process. This offers the possibility of creating a digital twin fusing machine data, sensor data, and simulation results to create a predictive tool for quality control. This manuscript presents the approach to creating a digital twin of the laser beam melting process. The first results for single-bead deposits are promising and show the potential of establishing a digital twin on process and quality control.

Overall, the huge potential of additive manufacturing of challenging alloy systems for high-tech applications was shown. The specifics of various additive manufacturing processes

require at least modifications to alloy systems and heat treatment routines developed for conventional manufacturing methods. In the opinion of the authors, the full potential of additive manufacturing can only be exploited if tailored alloys are developed. Unique microstructural features in additively manufactured parts due to the complex time-temperature history also require novel heat treatments. Herein, computational and high-throughput approaches offer significant advantages over conventional strategies in alloy development and heat treatment design.

Acknowledgments

The study "Laser powder bed fusion of copper-tungsten composites for use in power electronics" was funded by the German Federal Ministry of Economics and Climate Protection (BMWK) as part of the AiF-IGF program as part of a transnational CORNET project (No. 250 EN) based on a resolution by the German Bundestag. Simon Rauh thanks his team at Fraunhofer UMSICHT Lioba Fischer, Shashank Deepak Prabhu, and Gerhard Wolf for their support.

TUM and Oerlikon AM Europe GmbH would like to thank the TUM-Oerlikon Advanced Manufacturing Institute for the support of the research. Oerlikon AM Europe GmbH would like to thank for the support by the Bayerisches Staatministerium für Wirtschaft, Landesentwicklung und Energie (grant number NW-1901-0012) as part of this study.

References

[1] Derekar K S 2018 *Materials Science and Technology* **34** 895–916
[2] DebRoy T, Wei H, Zuback J, Mukherjee T, Elmer J, Milewski J, Beese A, Wilson-Heid A, De A and Zhang W 2018 *Progress in Materials Science* **92** 122–224
[3] Huang S H, Liu P, Mokasdar A and Hou L 2013 *The International Journal of Advanced Manufacturing Technology* **67** 1191–1203
[4] Yakout M, Elbestawi M A and Veldhuis S C 2018 *Solid State Phenomena* **278** 1–14
[5] Leino M, Pekkarinen J and Soukka R 2016 *Physics Procedia* **83** 752–760
[6] Subramanian P R and Laughlin D E 1991 Cu-W (Copper-Tungsten) *Phasen Diagrams of Binary Tungsten Alloys* ed Nagender Naidu S V and Rama Rao P (Calcutta: Indian Institute of Metals) pp 76–79 ISBN 978-8185307107
[7] Wang Y, Zhuo L and Yin E 2021 *International Journal of Refractory Metals & Hard Materials* **100** 105648
[8] Duan J, Guo X, Huang T, Song K, Feng J, Wang X, Zhong J, Duan K and Zhang Y 2023 *Materials Today Communications* **34** 105173
[9] Shao Y, Liu Y, Wu D, Song Z, Guo F and Zou Y 2023 *International Journal of Refractory Metals & Hard Materials* **115** 106315
[10] Wang C C and Lin Y C 2009 *International Journal of Refractory Metals & Hard Materials* **27** 872–882
[11] Liu T, Han Y, Jia D, Pang Z, Fu Y, Song Z and Ding Y 2024 *Applied Sciences* **14** 2731
[12] Rape A, Chanthapan S, Singh J and Kulkarni A 2011 *Journal of Material Science* **46** 94–100
[13] Tejadoa E, Müller A, You J and Pastora J 2018 *Materials Science & Engineering A* **712** 738–746
[14] v Müller A, Böswirth B, Cerri V, Greuner H, Neu R, Siefken U, Visca E and You J H 2020 *Physica Scripta* **2020** 014015
[15] Dong L L, Ahangarkani M, Chen W G and Zhang Y S 2018 *International Journal of Refractory Metals & Hard Materials* **75** 30–42
[16] Gu D and Shen Y 2009 *Journal of Alloys and Compounds* **473** 107–115
[17] Li R, Shi Y, Liu J, Xie Z and Wang Z 2010 *The International Journal of Advanced Manufacturing Technology* **48** 597–605
[18] Zhang D, Cai Q, Liu J, He J and Li R 2013 *The International Journal of Advanced Manufacturing Technology* **67** 2233–2242
[19] Yan A, Wang Z, Yang T Wang Y and Ma Z 2017 *The International Journal of Advanced Manufacturing Technology* **90** 657–666
[20] Wang M, Li R, Yuan T Chen C, Zhang M, Weng Q and Yuan Y 2018 *International Journal of Refractory Metals & Hard Materials* **70** 9–18
[21] Yan A, Wang Z, Yang T, Wang Y and Ma Z 2016 *Materials & Design* **109** 79–87
[22] Qin Y, Wu B, Wang G, Song P, Förster D J, Huang M and Yang S 2023 *Optics & Laser Technology* **162** 109243

[23] Zheng R, Li S F, Misra R D K, Kondoh K and Yang Y F 2023 *Journal of Materials Processing Technology* **322** 118169
[24] Li G, Brodu E, Soete J, Wei H, Liu T, Yang T, Liao W and Vanmeensel K 2021 *Additive Manufacturing* **47** 102210
[25] Rometsch P A, Zhu Y and Xinhua Wu and A H 2022 *Materials & Design* **219** 110779
[26] Martin J H, Yahata B D, Hundley J M, Mayer J A, Schaedler T A and Pollock T M 2017 *Nature* **549** 365–369
[27] Mishra R S and Thapliyal S 2021 *Materials & Design* **204** 109640
[28] Riener K, Nagler Aand Letofsky-Papst I and Leichtfried G 2022 *Alloys* **132** 277–287
[29] Uddin S Z, Murr L E, Terrazas C A, Morton P, Roberson D A and Wicker R B 2018 *Additive Manufacturing* **22** 405–415
[30] Guercio G D, McCartney D, Aboulkhair N, Robertson S, Maclachlan R, Tuck C and Simonelli M 2022 *Additive Manufacturing* **54** 102776
[31] Nie X, Chen Z, Qi Y, Zhang H, Zhang C, Xiao Z and Zhu H 2022 *Virtual and Physical Prototyping* **15** 325–339
[32] Kumar N S, Dhruthi, Pramod G, Samrat P and Sadashiva M 2022 *Materials Today: Proceedings* **58** 71–79
[33] Pereira J C, Gil E, Solaberrieta L, San Sebastián M, Bilbao Y and Rodríguez P P 2020 *Materials Science and Engineering: A* **778** 139124
[34] Mehta B, Frisk K and Nyborg L 2022 *Journal of Alloys and Compounds* **920** 165870
[35] Opprecht M, Roux G, Garandet J P and Flament C 2022 *Journal of Materials Engineering and Performance* **32** 1840–1855
[36] Pauzon C, Buttard M, Després A, Charlot F, Fivel M, Chehab B, Blandin J J and Martin G 2023 *Acta Materialia* **258** 119199
[37] Attallah M M, Jennings R, Wang X and Carter L N 2016 *MRS bulletin* **41** 758–764
[38] Risse J 2019 *Additive manufacturing of nickel-base superalloy IN738LC by laser powder bed fusion* PhD thesis Rheinisch-Westfälische Technische Hochschule Aachen Aachen URL `https://publications.rwth-aachen.de/record/764478`
[39] Song H, Lam M, Chen Y, Wu S, Hodgson P, Wu X, Zhu Y and Huang A 2022 *Journal of Materials Science & Technology* **112** 301–314
[40] Messé O, Muñoz-Moreno R, Illston T, Baker S and Stone H 2018 *Additive Manufacturing* **22** 394–404
[41] Peachey D D, Carter C P, Garcia-Jimenez A, Mukundan A, Leonard D N, Charpagne M A and Cordero Z C 2022 *Additive Manufacturing* **60** 103198
[42] Vogekpoth A, Sharma S and Schleifenbaum J H 2018 Development of Adapted Ni-738 Powder for Additive Manufacturing *Euro PM2018 proceedings: 14-18 October 2018, Bilbao Exhibition Centre (BEC), Bilbao, Spain / Euro PM2018 Congress & Exhibition; European Powder Metallurgy Association* (Shrewsbury, United Kingdom: European Powder Metallurgy Association (EMPA)) URL `https://publications.rwth-aachen.de/record/751611`
[43] MetcoAdd™ Metal Powder Portfolio for Additive Manufacturing last viewed 2024-06-14 URL `https://www.oerlikon.com/ecoma/files/AMPowderPortfolioflyer.pdf`
[44] Svetlizky D, Das M, Zheng B, Vyatskikh A L, Bose S, Bandyopadhyay A, Schoenung J M, Lavernia E J and Eliaz N 2021 *Materials Today* **49** 271–295
[45] Ahn D G 2021 *International Journal of Precision Engineering and Manufacturing-Green Technology* **8** 703–742
[46] Mykoniatis K and Harris G A 2021 *Journal of Intelligent Manufacturing* **32** 1899–1911
[47] Tao F, Cheng J, Qi Q, Zhang M, Zhang H and Sui F 2018 *The International Journal of Advanced Manufacturing Technology* **94** 3563–3576
[48] Lu Y, Liu C, Wang K I K, Huang H and Xu X 2020 *Robotics and Computer-Integrated Manufacturing* **61** 101837
[49] Gaikwad A, Yavari R, Montazeri M, Cole K, Bian L and Rao P 2020 *IISE Transactions* **52** 1204–1217
[50] DebRoy T, Zhang W, Turner J and Babu S S 2017 *Scripta Materialia* **135** 119–124
[51] Mukherjee T and DebRoy T 2019 *Applied Materials Today* **14** 59–65
[52] Gunasegaram D R, Murphy A B, Barnard A, DebRoy T, Matthews M J, Ladani L and Gu D 2021 *Additive Manufacturing* **46** 102089
[53] Hartmann S, Murua O, Arrizubieta J I, Lamikiz A and Mayr P 2024 *Simulation Modelling Practice and Theory* **132** 102881
[54] Chen L, Bi G, Yao X, Tan C, Su J, Ng N P H, Chew Y, Liu K and Moon S K 2023 *Robotics and Computer-Integrated Manufacturing* **84** 102581
[55] Hartmann S, Vykhtar B, Möbs N, Kelbassa I and Mayr P 2024 *Processes* **12** 1180
[56] Zou R, Liang X, Chen Q, Wang M, Zaghloul M A S, Lan H, Buric M P, Ohodnicki P R, Chorpening B, To A C and Chen K P 2020 *Journal of Lightwave Technology* **38** 6402–6411

[57] Hermann F, Chen B, Ghasemi G, Stegmaier V, Ackermann T, Reimann P, Vogt S, Graf T and Weyrich M 2022 *Procedia CIRP* **107** 83–88
[58] Karkaria V, Goeckner A, Zha R, Chen J, Zhang J, Zhu Q, Cao J, Gao R X and Chen W 2024 *Journal of Manufacturing Systems* ISSN 0278-6125
[59] Feng A, Chen C, Wu C, Wei Y and Wang Y 2022 *Metals* **12** 169
[60] Figueroa B S, Araújo L and Alvares A 2024 Development of a digital twin for a laser metal deposition (lmd) additive manufacturing cell *Advances in Automation and Robotics Research* (*Lecture Notes in Networks and Systems* vol 940) ed Cardona M N, Baca J, Garcia C, Carrera I G and Martinez C (Cham: Springer Nature Switzerland) pp 68–76 ISBN 978-3-031-54762-1
[61] Kaufman L and Bernstein H 1970 *Computer Calculation of Phase Diagrams* (Academic Press NY) ISBN 0-12-402050-X
[62] Olson G and Liu Z 2023 *Calphad* **82** 102590
[63] Kattner U R 2016 *Tecnol. Metal. Mater. Min.* **13** 3–15
[64] Wang X and Xiong W 2020 *npj Computational Materials* **6** 188
[65] Carrion Ständer S, Barschkett N and Kabliman E 2023 *Integrating Materials and Manufacturing Innovation* **12** 289–300
[66] Matcalc: Matcalc—solid state and kinetics precipitation last viewed 2024-06-14 URL `https://www.matcalc.at/`